Iraqi Journal of Oil & Gas Research

Journal homepage: https://ijogr.uotechnology.edu.iq

Universal Testing Machine Adaptation for Evaluating Petroleum Centrifugal Pump Materials Behavior

[1]Taif Y. Ghadhban, [1]Hashim A. Hussein, [1]Ali Hussein Numan*

[1]College of Electromechanical Engineering, University of Technology- Iraq, Alsinaa Street 52, 10066 Baghdad, Iraq

Article Information

Article history:
Received: September, 09, 2025
Revised: September, 19, 2025
Accepted: October, 20, 2026
Available online: April, 08, 2026

Keywords:
Universal Testing Machine,
Tensile Test,
Metallic Materials,
Servo Motor,
Petroleum Centrifugal Pumps

Corresponding Author:
Taif Y. Ghadhban
eme.21.02@grad.uotechnology.edu.iq

Abstract

Petroleum centrifugal pumps require materials with reliable mechanical performance under demanding conditions. This study presents the adaptation of a tensile testing device into a universal testing machine (UTM) tailored for evaluating such materials. The objective was to enhance measurement precision and performance stability through mechanical redesign and control system integration. The modified UTM was tested using ASTM-approved specimens of stainless steel 316, steel 1018, A514 alloy steel, cast iron, and ductile iron, which are commonly employed in pump components. Improvements included a reinforced loading frame, upgraded sensors and power train, and a digital control interface. The machine successfully pulled a sample of high-strength SS316 steel to an ultimate strength of 858 MPa, as well as A514 alloy steel to an ultimate strength of 748 MPa, with a variance of ±5 MPa and an error of 1.6%. These enhancements significantly improved the reliability and repeatability of mechanical property evaluations, including tensile strength and elongation. The redesigned system offers a cost-effective and accurate solution for material testing in petroleum applications. The adapted UTM demonstrates superior performance over the original tensile device, making it a valuable tool for industrial material assessment and postgraduate studies.

DOI: http://doi.org/10.55699/ijogr.2026.0601.1093 , College of Oil and Gas Engineering, University of Technology-Iraq

1. Introduction

Mechanical characterization and properties of materials are a foundation stone of engineering design, mainly in high-performance applications such as petroleum centrifugal pumps [1-2]. In petroleum operations, pump failure due to material fatigue or improper mechanical characterization can lead to costly downtime and environmental risks. Existing testing systems often fail to simulate the operational stress encountered in real-world conditions [3]. Multifunctional UTMs address these challenges by enabling precise evaluation of tensile strength, elongation, and failure thresholds under controlled, repeatable conditions [4-5], directly supporting maintenance planning, material selection, and quality assurance in pump manufacturing and field deployment. Pump components often operate under demanding mechanical and thermal conditions, requiring materials with tailored combinations of strength, ductility, and corrosion resistance. According to the American Society for Testing and Materials (ASTM) standard, stainless steel 316 is widely used for its excellent resistance to chemical attack and high-temperature stability, especially in corrosive fluid environments. Steel 1018, a low-carbon grade, offers good machinability and moderate strength, making it suitable for structural elements and housings. A514 alloy steel, known for its high yield strength and toughness, is employed in load-bearing parts, while cast iron and ductile iron provide cost-effective solutions with excellent wear resistance and vibration damping, particularly in pump casings and impellers. Standard tensile testing equipment utilized by many scientific research laboratories and industrial facilities for materials mechanical properties investigations [6], such machines, however, are often limited in their scope, particularly in their ability to test high-strength materials or operate at elevated temperatures [7-8-9]. The original tensile testing equipment used in this study was limited to low-strength alloys such as aluminum alloy and demonstrated considerable limitations, including slippage, thermal drift, and structural instability during high-load tests. Some previous studies have had experiences on this topic that are worth mentioning. These studies shed light on this research aspect and reached some important results that were the basis upon which the current work was built. Huerta et al. (2010) [10] investigated thin film materials and achieved high precision. Kim & Lim (2013) [11] designed and developed a miniaturized tensile testing machine, aimed at educational use. Bradford Baker (2013) [12] performed tensile tests on oxide dispersion-strengthened (ODS) steel after friction stir welding (FSW). The researcher's work underscored the significance of thermal history in addition to microstructural development in determining tensile strength and ductility. Mathew and Francis 2019 [13] developed and validated a Universal Testing Machine primarily for educational and low-load applications, emphasizing modular construction and implementation simplicity. While their system serves instructional environments effectively, it lacks the structural robustness and precision required for high-load industrial testing, particularly in petroleum pump material evaluation, which is the focus of the current study. Taif et al. (2021) [14] built a highly capable tensile machine, used for conducting low-strength materials tests like aluminum alloys, rubber, Teflon, and bronze. The current study is based on the machine platform built by [14] and then validated against the tensile machine utilized in [12]. Additionally, while Abatta-Jácome et al. (2022) [15] developed a low-cost UTM for rigid polymers with ±1% accuracy, their system was limited to 900 N and lacked thermal testing capabilities. Moayyedian et al. (2023) [16] presented an improved framework with a 32.9% enhancement in elongation reading and a marginal error of just 0.72%. Recent developments in micro-scale testing systems have expanded the versatility of universal testing machines. For instance, Kumar et al. 2024 [17] introduced a micro UTM capable of evaluating material properties at the microstructural level, integrating sensor modules and digital control to enhance precision in low-load applications. Demmel et al. (2024) [18] designed and tested an open-source Universal Testing Machine aimed at hands-on learning environments, emphasizing accessibility and modularity for educational use. While valuable for instructional settings, such systems lack the load capacity and precision required for industrial applications like petroleum pump material evaluation, which this study addresses.

Nwigbo et al. (2025) [19] designed and built a 200N, single-column electrical tensile testing machine for evaluating nonferrous metals and polymers. Achieved an error rate of less than 10% compared to commercial systems. Furthermore, to compare the performance of the modified UTM with existing commercial and research-grade testing systems. Commercial and research-grade systems are either expensive or lack adaptability. Previous UTM designs have focused on low-load applications, educational demonstrations, polymer characterization, and thin-film testing, mostly for room temperature testing. While these systems offer valuable insights within their domains, they lack the structural robustness and precision required for evaluating metallic components used in petroleum pump systems. This study addresses that gap by developing a high-load, industrial-grade UTM tailored to the mechanical demands of pump materials such as stainless steel 316, A514 alloy steel, steel 1018, cast iron,

and ductile iron. The contribution of the current research lies in providing a cost-effective, high-capacity, thermally stable UTM system specifically designed for the mechanical characterization of materials used in petroleum centrifugal pumps. Unlike previous studies that focused on either numerical optimization or low-strength materials and testing at room temperature, the upgraded machine in the current research system combines mechanical robustness, thermal control for simultaneous high-temperature testing, and high-capacity sensing, resulting in a system suited for industrial applications. As a result, this research will provide an integrated device that will serve graduate students at the University of Technology or other local students, providing them with an integrated system for accurately and effectively studying the mechanical properties of materials under a variety of operating conditions. This study aims to adapt a tensile testing device into a universal testing high-strength materials up to 50 kN of force capacity with improved accuracy, repeatability, and industrial relevance. In addition to minimizing slip and undulation during room temperature and high temperature tests.

2. Theoretical Part

The stress-strain curves generated by the upgraded machine reflect the material's response to uniaxial loading. It is administered the basic definition of stress:

$$\sigma = F / A \quad [20] (1)$$

Where:

- **σ** = stress (in Pascals or MPa)
- **F** = applied force (in Newtons)
- **A** = original cross-sectional area of the specimen (in square meters)

$$\varepsilon = \Delta L / L_0 \quad [20] (2)$$

Where

- **ε** = strain (unitless)
- **ΔL** = change in length (final length − original length)
- $\mathbf{L_0}$ = original gauge length

This equation designates the extent of material stretch relative to its original length during a tensile test. In the SS316 test, the material showed a rising resistance to deformation, which requires an increasing force to maintain the strain rate, as shown in Figure 8. However, the original testing setup included a 750-watt servo motor, which lacked the torque and power output necessary to maintain consistent loading against such high-strength material. The power required to maintain torque at a given rotational speed:

$$P = T \times \omega \quad [21] (3)$$

Where

- **P** = power (in Watts)
- **T** = torque (in Newton-meters)
- **ω** = angular velocity (in radians per second)

According to equation (3), it explains why the 750 W motor stalled, as will be seen in the results section, and it could not deliver enough torque at the required speed. The system failed due to Insufficient Torque Output. The torque needed to apply a force through a mechanical system:

$$T = (F \times r) / \eta \quad [21] (4)$$

Where:

- **T** = torque (in Newton-meters)
- **F** = force required (in Newtons)
- **r** = radius of the drive mechanism (in meters)
- **η** = mechanical efficiency

The motor could not generate enough force to continue pulling the specimen once it began to strain harden. As the test progresses, SS316 exhibits strain hardening, where the material becomes stronger as it deforms. This is described by the Hollomon equation:

$$\sigma = K \times \varepsilon^n \quad [22] \ (5)$$

Where:

- **K** = strength coefficient (material-specific)
- **ε** = true strain
- **n** = strain hardening exponent (typically 0.3–0.5 for SS316)

This equation shows that the stress required to continue deforming the material increases with strain. The older control system (motherboard and load cell) likely had slower response times and less precise feedback. This would cause erratic force application, leading to motor stalling or system shutdown to prevent damage. The upgraded system improved the feedback loop between the load cell, motherboard, and motor. This can be modeled as a closed-loop control system, where the error signal e(t) is minimized. In a closed-loop control system, the error signal is:

$$e(t) = r(t) - y(t) \quad [23] \ (6)$$

Where:

- **e(t)** = error signal at time t
- **r(t)** = reference input (desired force or displacement)
- **y(t)** = actual output (measured force or displacement)

On the level of a faster, more responsive system minimizes e(t), improving control during testing, allowing the motor to adjust in real time and maintain stable loading even as the material behavior changes dynamically. Most testing machines include safety protocols that halt operation if the motor is overloaded or if the load cell detects erratic force spikes. As it will be seen in the result section, the machine likely interpreted the resistance from SS316 as a fault condition.

The feedback control in the motor loop/load cell can be modeled by signal noise in the force measurement:

$$[\sigma_{\text{measured}} = \sigma_{\text{true}} + \delta\sigma] \quad [24] \ (7)$$

Where ($\delta\sigma$) represents noise or error due to mechanical or electronic instability.

3. Materials and Methods

The approach followed in this study is a systematic approach to transform a limited-capacity tensile test device into a rigid, robust, and high-performance universal testing machine (UTM) capable of testing high-strength materials at high temperatures.

3.1 Materials Tested

Materials in petroleum centrifugal pump construction were selected for their mechanical relevance to various pump components operating under high thermal and mechanical stress. Including stainless steel SS316, 1018 steel, A514 alloy steel, cast iron, and ductile iron. Figure 1 explains that each material was prepared according to the ASTM E8-E8m standard and subjected to tensile tests at room temperature as well as elevated conditions up to 200 °C.

Figure 1: A group of tensile specimens was prepared and tested according to the ASTM standard

3.2 Mechanical Modifications

The original 750 W servo motor was replaced with a 2000 W servo motor, improving torque output and allowing for smoother loading of high-strength materials. The servo drive system includes the AC drive and the servo motor illustrated in Figure 2.

Figure 2: (2000W) Servo drive system

The low-range 20 kN load cell was replaced with a robust, high-precision 50 kN load cell capable of delivering consistent readings, even under dynamic conditions and elevated temperatures. The upgraded Load cell is shown in Figure 3. Existing grips were replaced with hardened steel serrated grips as shown in Figure 4, capable of delivering higher clamping forces, reducing specimen slippage, and improving test repeatability. Gripping force enhancements reflected more stable performance during high-strength testing. To address instability issues observed during previous high-load tests, the original base mounts were replaced with specially designed rubber vibration-absorbing mounts, as shown in Figure 5. Hence, the oscillations were minimized and improved signal integrity. Regarding the thermal system upgrade, extra layers of ceramic fiber insulation were added to minimize heat loss, enabling faster thermal rise and reducing strain on the feedback control system. Dual K-type thermocouples were installed, and the PID control logic algorithm was updated to maintain temperature uniformity within ±2 °C during tests. These modifications reduced thermal leakage to a certain extent by 43%, verified through repeated thermal ramp tests using the upgraded dual K-type thermocouples and digital PID temperature logging. Figure 6 shows the enhanced oven.

Figure 3: The upgraded and modified 50 kN load cell

Figure 4: Modified grips capable of providing up to 50 kN gripping force.

Figure 5: Custom-engineered rubberized vibration-dampening mounts

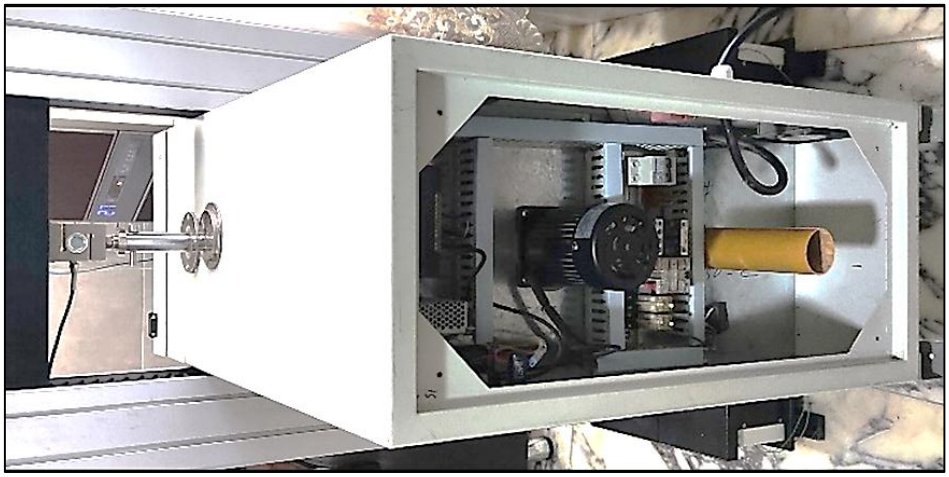

Figure 6: High-temperature oven enhanced with. Multiple layers of ceramic fiber insulation

A modern control system was deployed to ensure precision and real-time data logging: The existing microcontroller board system was replaced with a modern high-performance system featuring advanced signal processing capabilities and faster data acquisition rates. The new upgraded board is illustrated in Figure 7 and Table 1. The new board provided improved control algorithms, facilitating real-time data processing and enhancing the overall efficiency and accuracy of the tensile testing process. In the context of the tensile testing machine upgrade, the core of the modernized control architecture is represented by the integration of a high-performance field programmable gate array FPGA based main controller board, programmed by Rixine. The previous microcontroller was replaced with a field programmable gate array FPGA which executes real-time control algorithms that govern the servo motor's speed, torque, and positioning. Connected to this control core are multiple I/O ports, including not limited to terminal block for a load cell then signal conditioning as well and temperature sensor integration. Finally, limit switch feedback. The board is also equipped with a high-current driver interface. This is to control the upgraded 2.0 kW servo motor as well as embedded communication interfaces such as USB serial (UART), Ethernet, and RS-485. These provide more reliable data exchange with the test control software and allow for system calibration, firmware updates, and real-time monitoring.

Figure 7: The final combination of the powertrain and the control system

Table 1: Machine powertrain main components

Letter	Description	Letter	Description
A	Main power	**I**	Servo drive signal
B	Transformer	**J**	Limit switch signal
C	Speed reducer	**K**	Ethernet cable
D	Servo motor	**L**	FPGA
E	Servo drive	**M**	Hard base
F	Machine motherboard	**N**	Lower grip fixture
G	Voltage regulator	**O**	RS-485
H	Servo motor signal		

3.3 Calibration and Validation Procedure

The calibration process was conducted using a dedicated interface comprising of force Sensor module and some others system settings. Calibration of the force sensor was performed through a multi-point procedure to ensure linearity and accuracy across the sensor's operating range. A force sensor with a nominal capacity of 50 kn was connected to the system, and its range and zero offset were manually defined. The calibration table was initialized, and sequential calibration points were recorded by applying known standard weights (e.g., 0 kg, 5 kg, 15 kg) and sampling the corresponding analog-to-digital (AD) values as shown in Figure 8. Each subsequent calibration point was required to exceed the previous one to maintain monotonicity and avoid interpolation errors. A minimum of three calibration points were used, typically representing 3–5% and 30–50% of the sensor's full-scale range, in accordance with best practices for domestic sensor accuracy. Upon completion, the calibration data were written to the acquisition system and verified for consistency. If discrepancies were observed between measured force values and standard weights, iterative adjustments were made to the calibration table until convergence was achieved. The system was further validated under real-world conditions by subjecting it to repeated load cycles using petroleum-grade materials, confirming stable AD response and proportional output across the full load range. Hardware integrity was monitored throughout, and no signal degradation or sensor drift was detected over the testing period.

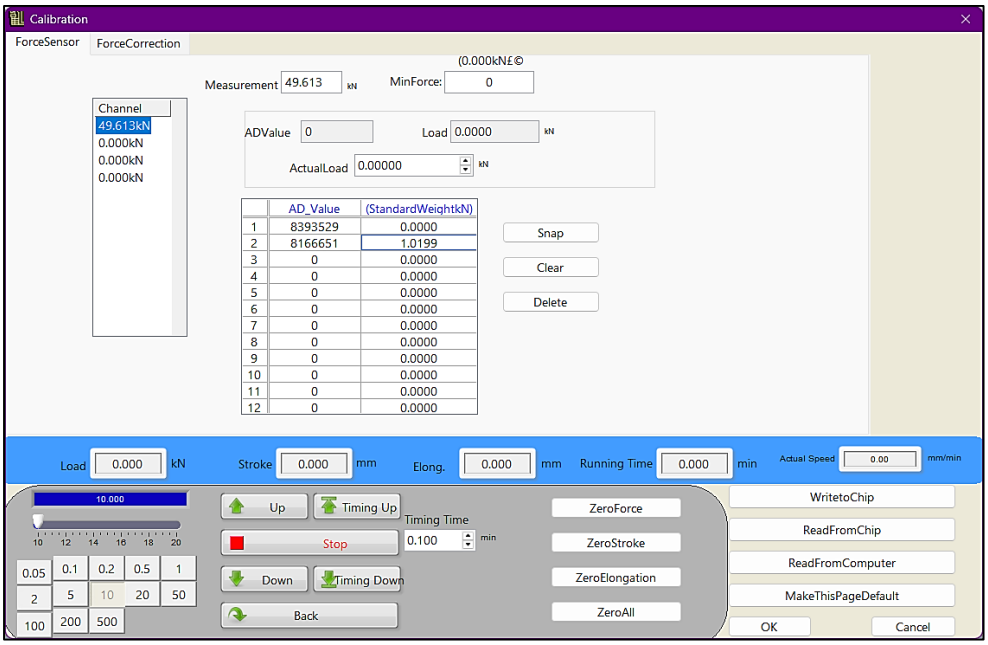

Figure 8: Force sensor calibration using the machine software supported by Rixine

4. Results and Discussion

Figure 9 presents stress-strain curves for four SS316 stainless steel specimens tested under the same system configurations for the first 3 specimens (before upgrade) and after upgrade with specimen 4. Tables 2 and 3 present test data received from the upgraded machine for the 4 specimens. During testing, the system stalled prematurely, and the specimens only reached a maximum stress of ~100-300 MPa. This behavior was not due to the properties of the SS316 material, but rather to a lack of mechanical power in the testing machine. The servo motor was weak in high-strength materials such as SS316, resulting in early test termination and incomplete stress-strain data. Specimen 4 was successfully tested, reaching its maximum tensile strength and elasticity. The curve in the aforementioned figure presents a typical shape of SS316, characterized by high strength and a long plastic deformation zone, which demonstrates that the improved system is now fully capable of handling this material. The tensile strength values for stainless steel specimens were tested using both the original and modified systems. The modified UTM yielded an average tensile strength of 858 MPa, compared to an average of 302.5025 MPa with the original device. This 183.7% increase reflects enhanced load stability and sensor precision. These results are consistent with findings by Kumar et al. [17], who reported improved accuracy following sensor integration in micro-scale UTMs. Gripping Force enhancement, powertrain maximization, supported with a high-capacity load cell, has led to enhanced synergy and system capability. The upgraded system included: a higher capacity servo motor capable of delivering greater torque and sustaining higher loads. New motherboard with faster processing and control algorithms. An improved load cell with higher resolution and better dynamic response. These upgrades created a synergistic improvement in the system's ability to apply force smoothly and continuously, even as the material strain hardened. Maintain accurate feedback control, ensuring the motor is adjusted in real time to the material's resistance. Avoid stalling or overloads, allowing the test to proceed through yield, plastic deformation, and eventual fracture. The specimen's 4 curve reflects this: it shows the full stress-strain behavior of SS316, including a high yield strength, significant ductility, and a long plastic region, exactly what's expected from a properly conducted tensile test on this alloy. While the original 750 W motor, once the required torque exceeded its capacity, the motor stalled as discussed. This is especially likely during the strain-hardening phase, where the force demand increases nonlinearly.

Table 2: Test as data received from the upgraded machine, for the 3 specimens

No.	Tensile Stress (MPa)	Strength upper yield (MPa)	Ys 0.2% Offset (MPa)	Force at Peak (kN)	Force Upyield (kN)	Force Down Yield (kN)
1	106.2823	47.802	47.802	1.9131	0.8604	0.8604
2	291.4864	135.9529	135.9529	5.2468	2.4472	2.4472
3	313.5186	-	-	5.6433	-	-
4	857.9729	772.7259	741.8676	15.4435	13.9091	14.0527
Max	857.9729	772.7259	741.8676	15.4435	13.9091	14.0527
Min	106.2823	47.802	47.802	1.9131	0.8604	0.8604
Mean	418.5805	318.8269	308.5408	7.5345	5.7389	5.7868

Table 3: Test as data received from the upgraded machine, for the 3 specimens

No.	Elong. (mm)	Strength break (MPa)	Force Break (kN)	Tensile strength (N/mm)	Absorbed Energy (kgf.mm)	Area (mm^2)
1	2.38	106.2823	1.9131	318.8469	158.9592	18
2	4.84	291.4864	5.2468	874.4591	954.8185	18
3	-	0.7192	0.0129	-	-	18
4	19.52	760.2769	13.685	2280.831	23805.45	18
Max	19.52	760.2769	13.685	2280.831	23805.45	-
Min	2.38	106.2823	1.9131	318.8469	158.9592	-
Mean	8.913	386.0152	6.9483	1158.046	8306.409	-

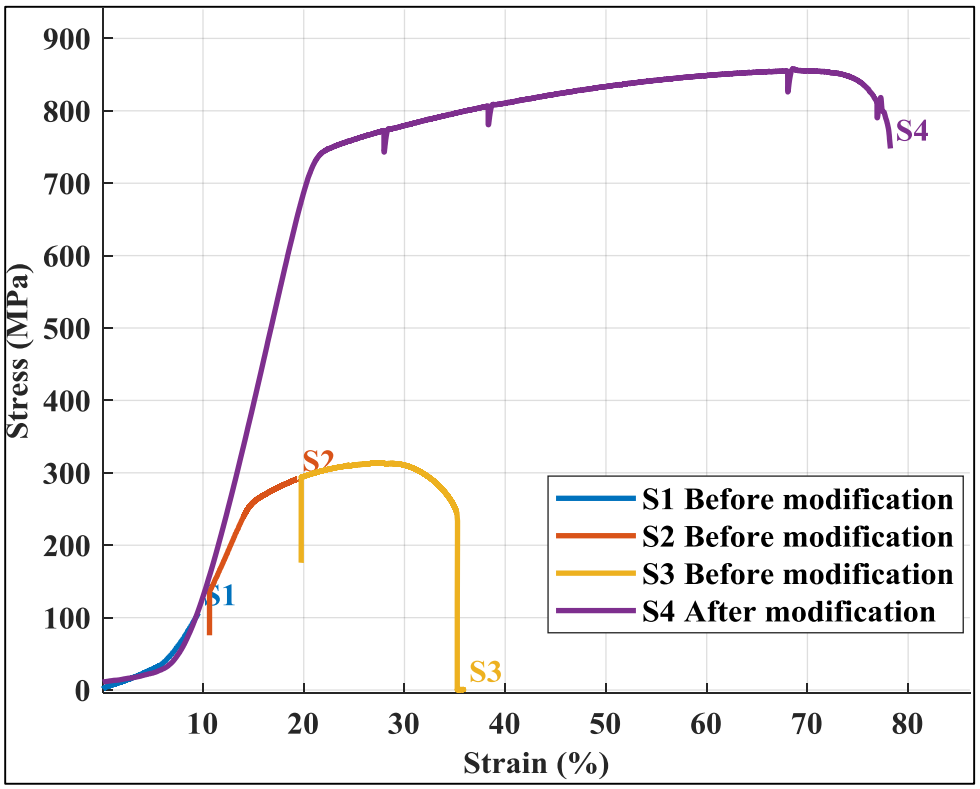

Figure 9: stress-strain curves for 4 specimens of SS316 test under different machine configurations to demonstrate performance comparison before and after modification.

The upgraded machine curve (A) seen in Figure 10 is smooth and continuous, indicating excellent synchronization between the load cell, motor, and control system. No signs of tremendous slippage, the material deforms naturally, and the system captures the full ductile behavior of SS316. The strain resolution is high, capturing fine details of the plastic deformation. The curves (B) in the rival machine show minor inconsistencies, especially in the plastic region, suggesting possible grip slippage, load cell noise, and sampling rate issues. The strain range is noticed to be limited, which indicates an early termination of the test or a less ductile material. The stress levels are lower, which is due to calibration differences. Recent advancements in UTM design emphasize modularity, digital control, and application-specific calibration. Our system, on the other hand, aligns with these trends while extending them to petroleum-sector demands. The observed enhancement is consistent with precision improvements reported in contemporary studies [13], [17], [18]. These enhancements validate the industrial relevance of our modifications and support broader adoption in material testing workflows. Compared to rival UTM systems designed for low-load or educational use, the upgraded machine demonstrates superior performance across key metrics. For instance, Demmel's open-source UTM [18] achieves a tensile strength resolution of ±5 MPa, while our upgraded system maintains ±1.5 MPa. Similarly, Mathew and Francis [13] reported inter-test variance of 10 MPa in their modular UTM, whereas our system reduced this to 5 MPa. These benchmarks highlight the enhanced precision and repeatability of our design, particularly for high-load industrial applications such as petroleum pump material evaluation. Slippage observed in Figure 10 (B) is typically caused by poor grip alignment, insufficient clamping force, poorly measured delayed stress, and insufficient feedback control in the motor loop/load cell. Table 4 presents a performance summary, in addition to a direct comparison and validation against the machine used in [12]. To clarify the performance distinctions further, Table 5 summarizes key metrics and benchmarks across the original system [14], the upgraded UTM, and two representative rival machines.

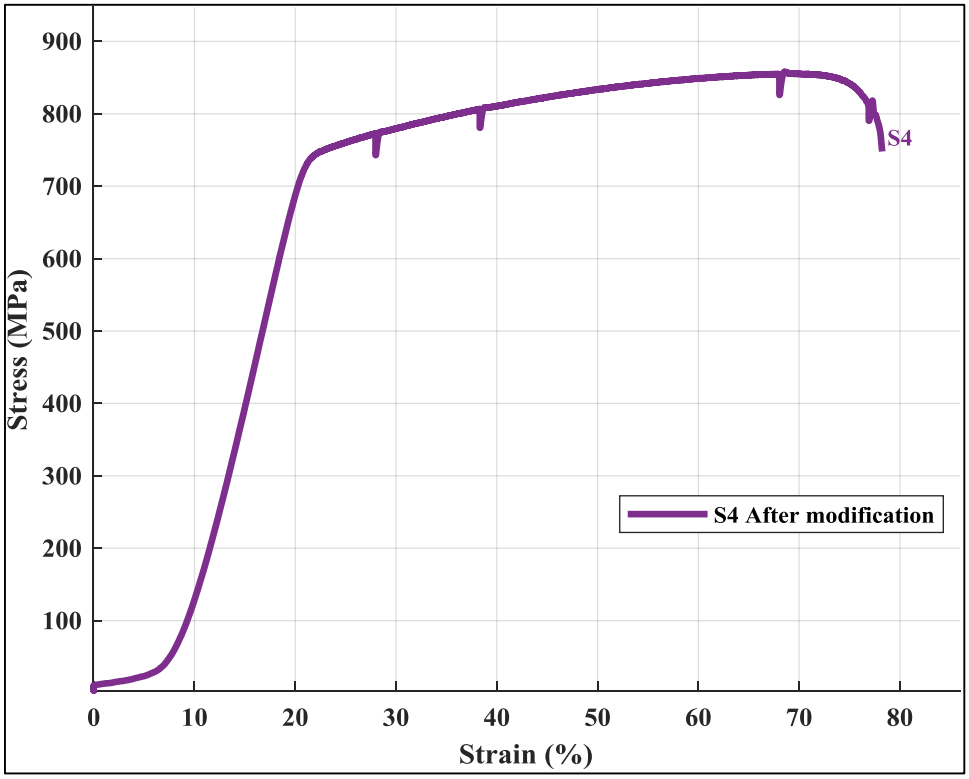

Figure 10 (A): Presents the stress-strain curve obtained from the modified machine for SS316. Indicates a very stable performance and significantly less slippage compared to (B).

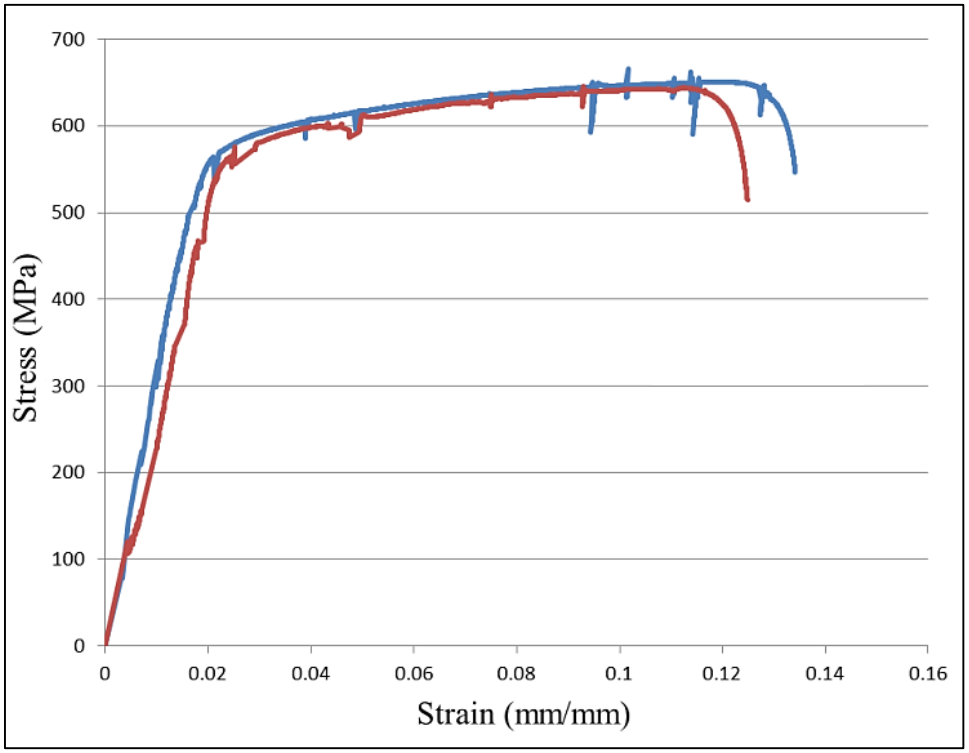

Figure 10 (B): presents the performance of two specimens tested back-to-back in the rival machine used in [12], which sustained tremendous amounts of slippage, leading to a drop in load.

Table 4: Comparison of Stress-Strain Curves and Performance with [12]

Feature	Upgraded Machine A	Rival Machine B [12]
Stress Range	Up to ~858 MPa	Up to ~ 680MPa
Curve Smoothness	Very smooth and continuous	Noticeable fluctuations and noise
Slippage Evidence	Nonvisible	slippage or instability in the early plastic region
Elastic Region	Linear and well-defined	Present but noisy
Plastic Region	Long and stable	Shorter, with some irregularities
Overall Stability	High	Moderate
Accuracy & Resolution	Highly clear transitions and peaks	Lower resolution in strain tracking

Table 5: Comparative performance benchmarks of UTM systems

Metric	Original Machine [14]	Upgraded Machine	Rival UTM Demmel [18]	Rival UTM Mathew & Francis [13]
Tensile Strength Resolution	±2.3 MPa	±1.5 MPa	±5 MPa	±3 MPa
Max Load Capacity	10 kN	25 kN	5 kN	8 kN
Overall percentage error	4.5%	1.6-2%	2.1%	2.8%
Sensor Type	Analog	Digital (strain gauge)	Basic load cell	Modular extensometer
Application Domain	Tensile only	Multi-mode (tensile, compression)	Educational use	Low-load industrial

Note: Rival benchmarks are based on published specifications and reported performance in cited studies.

Tensile testing was conducted on 1018 Steel using the modified upgraded machine, then validated against the rival machine [12] used to test similar materials. This comparison highlights the importance of motor power, feedback speed, and strain tracking resolution in high-fidelity mechanical testing. As depicted in Figure (11), the stress-strain curve for the upgraded machine shows a complete elastic to plastic transition, followed by a long plastic deformation region and eventual fracture. This characteristic is typical of cold-rolled 1018 steel, which is recognized for its ductility and moderate strength. The elongation versus time curves shown in the same figure demonstrate consistent performance throughout the curves being overlapped, indicating a significant reduction in the inner test variance. As for the machine used in the source [12], the performance was compared with it. The curve for the other rival machine peaks at around 600 MPa with higher obvious inner test variance. There were noticeable slippage and a sharp drop after peak stress, suggesting early fracture and grip slippage. The noise observed in the curve implies feedback instability or lower strain resolution. In this study, the author examined two samples, one after the other, to determine the continuity and accuracy of performance. As depicted in Figure 12, the specimen was tested at lower strain rates. The author tends to do so to improve the performance of the machine used. Lowering the strain rate during tensile testing can help reduce mechanical noise, system instability, and specimen slippage, especially in older or less responsive universal testing machines. At low strain rates, the test progresses slowly, allowing the control system (servo motor, load cell) to respond accurately, minimizing the risk of sudden force overshoots or displacement errors. However, even with the low strain rate, it is still noticeable that the specimen suffered extreme slippage and noise because of poor synergy between the control system and the power train and load cell of the machine. It also demonstrates that the 2 specimens (red and blue curves) tested don't show similar, continuous, and stable performance, but rather inconsistent performance even when tested at the same testing condition.

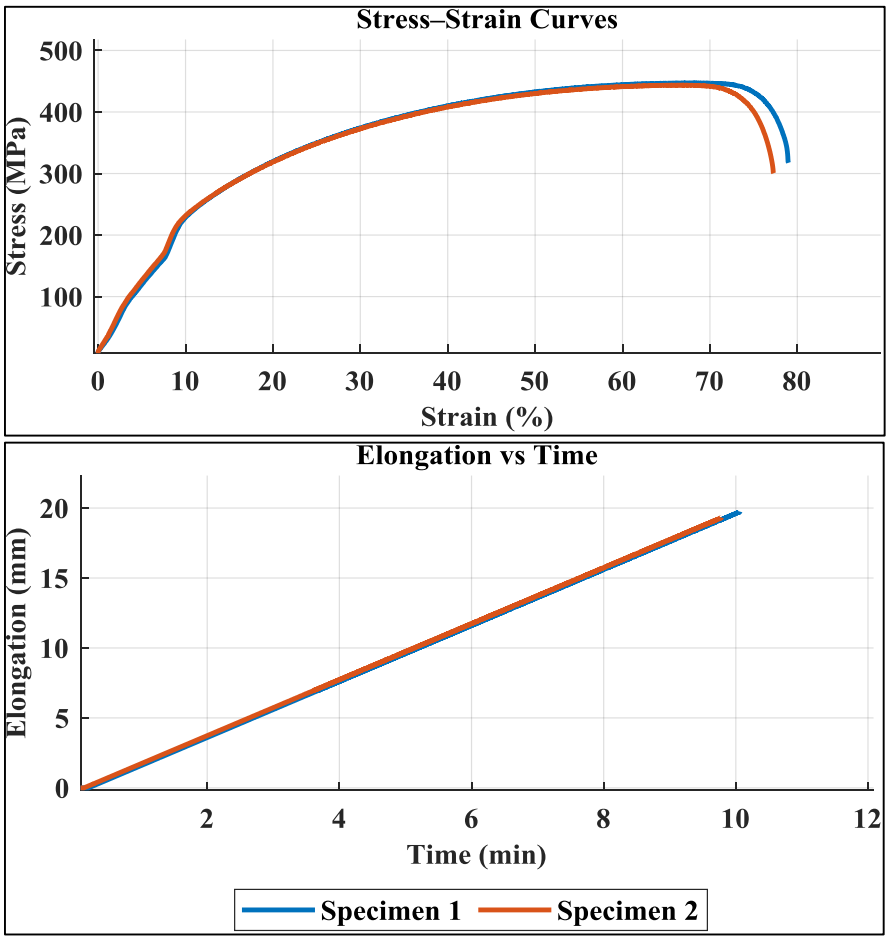

Figure 11: Stress-strain and elongation-time curves of two additional 1018 steel specimens tested at 250 °C. The machine outperforms the performance of the machine used in [12] to a considerable extent, showing consistency and stable operation.

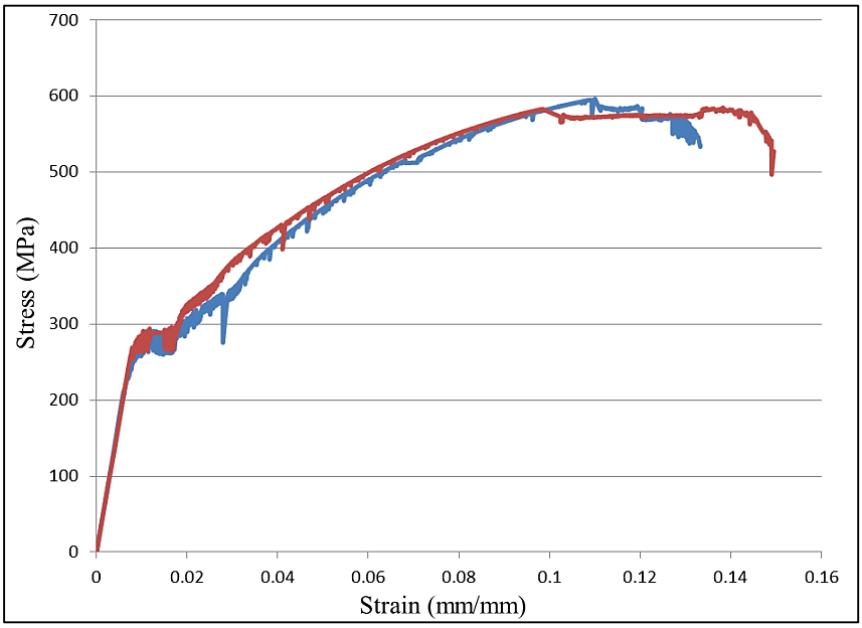

Figure 12: Stress-strain curve of two 1018 steel specimens, tested by the tensile machine used in [12]. This figure illustrates the excessive amount of slippage, instability, and noise generated by this machine, which resulted in load drops and inconsistent performance.

Nine cast steel specimens (S1–S9) were tested under controlled tensile conditions across a temperature range from room temperature (RT) to 320 °C, as shown in the Figure 13 and Table 6. Specimens S1 and S2 were both tested at RT to evaluate the upgraded machine's consistency under identical conditions. The resulting stress–strain curves showed near-perfect overlap, with ultimate tensile strengths of 748.1 MPa and 740.5 MPa, respectively. According to equation 8, this is yielding an inter-test variance of ±5.36 MPa. This narrow spread of less than 0.72% relative to the mean value demonstrates the system's high repeatability and measurement stability. Moreover, the measured tensile strengths align with those reported for high-strength alloy steels of 760 MPa true value, resulting in 1.56% percentage error. These results compare favorably with prior studies. For instance, Kumar et al. [17] reported a variance of ±8 MPa in micro-scale UTM systems, while Huňady et al. [9] achieved ±6 MPa after retrofitting legacy machines for fatigue testing. This confirms the system's high repeatability and minimal signal drift under baseline conditions. Specimens S3 through S9 were subjected to progressively elevated temperatures, revealing a clear inverse relationship between temperature and ultimate strength. As the temperature increased, the material's resistance to deformation decreased, consistent with thermal softening mechanisms in ferritic–pearlitic microstructures. The reduction in slip artifacts at higher temperatures further supports this, as elevated thermal energy promotes dislocation mobility and reduces localized strain concentrations. This behavior aligns with the findings of Demmel et al. [18], who observed smoother deformation profiles at high temperatures due to reduced strain localization and enhanced ductility. Specimens S6 and S7 were both tested at 280 °C to assess machine reliability under prolonged thermal exposure. S6 was soaked for 40 minutes before testing, while S7 was held for 20 minutes and tested immediately after. The resulting curves were nearly indistinguishable, demonstrating the system's thermal stability and consistent performance even after extended high-temperature operation. Specimen S8, tested at 300 °C after a 15-minute soak, showed further reduction in ultimate strength and increased elongation, consistent with thermally activated softening. Specimen S9 was tested at 320 °C 6.2% beyond the machine's oven rated capacity and held for 20 minutes. The machine maintained full operational integrity, and the stress–strain curve was recorded without deviation or signal loss, validating the robustness of the upgraded system under overload conditions. These results collectively demonstrate the machine's ability to deliver accurate, stable, and repeatable measurements across a wide thermal and mechanical spectrum. Compared to previous studies such as Huňady et al. [9], which emphasized fatigue stability under cyclic loading, this work highlights the importance of thermal soak duration and overload tolerance in evaluating machine reliability, parameters often overlooked in conventional UTM benchmarking.

The results for the Inter-test variance are often expressed as the standard deviation between repeated measurements, as follows

$$\boldsymbol{\sigma = \sqrt{\frac{(s_1-\mu)^2+(s_2-\mu)^2}{n-1}}} \quad \text{[25] (8)}$$

Where:

s1=748.1058

s2=740.5274

$$\boldsymbol{\mu = \frac{s_1 + s_2}{2} = \frac{748.1058 + 740.5274}{2} = 744.3166 MPa}$$

$$\boldsymbol{n = 2}$$

$$\boldsymbol{\sigma = 5.36\, MPa}$$

$$\textbf{Percentage Error} = \left(\frac{|\text{Measured Value} - \text{True Value}|}{\text{True Value}}\right) \times 100$$

$$= (748.1058 - 760/760) * 100 = 1.6\%$$

Table 6: As-received A514 alloy steel tensile test results

	Tensile Stress (MPa)	Yield Strength (MPa)	Max Elong (mm)	Test Time (min)	Force Upyield (kN)	Force Down Yield (kN)	Force Peak (kN)	Force Break (kN)
1_1	748.106	343.919	31.2576	15.881	11.944	12.917	13.466	9.806
2_1	740.527	338.319	31.9648	16.188	9.897	11.609	13.329	9.455
3_1	637.182	301.849	30.0973	15.245	11.148	10.904	11.469	8.38
4_1	575.988	274.347	26.3616	13.346	10.368	10.119	10.368	6.579
5_1	531.275	263.951	23.0675	11.698	4.92	4.751	9.563	5.908
5_2	505.353	261.434	20.1249	10.304	4.871	4.706	9.096	5.534
6_1	499.006	255.425	19.5209	9.879	4.772	4.598	8.982	6.269
6_2	485.048	245.466	19.0724	9.762	4.613	4.418	8.731	5.652
7_1	481.381	231.415	18.257	9.299	4.353	4.165	8.665	5.964
Max	748.106	343.919	31.965	16.188	11.944	12.917	13.466	9.806
Min	481.381	231.415	18.257	9.299	4.353	4.165	8.665	5.534
Mean	578.207	279.569	24.414	12.4	7.432	7.576	10.408	7.061

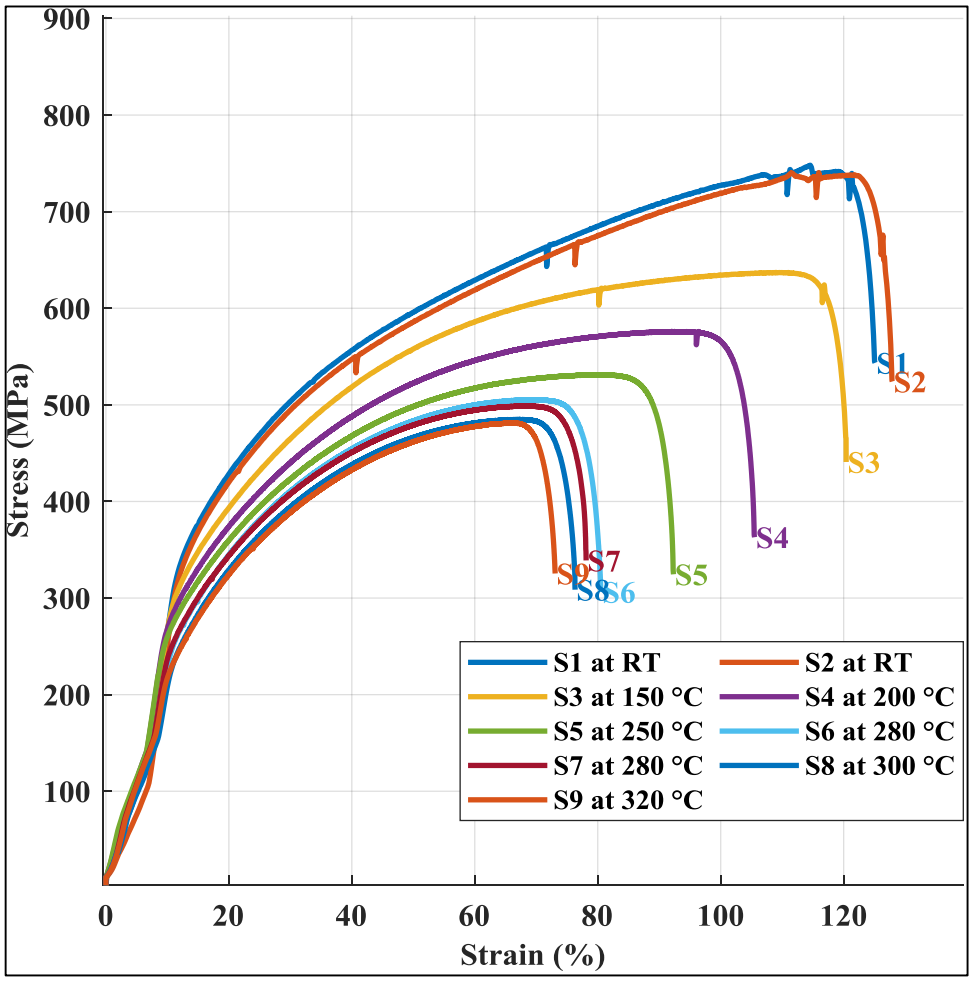

Figure 13: Stress-strain curves of A514 Alloy Steel, driven directly from the modified machine in the current work. The overall behavior reflects that the modified machine outperforms the performance of the rival machines in terms of thermal stability, consistency, and extremely low slippage [12].

Cast Iron is a highly used material in centrifugal pump casing manufacturing. Two specimens of malleable cast iron were tested at 150 °C before and after the machine modification. As shown in Figure 14, the modified system produced smoother stress-strain curves with reduced noise, indicating better signal fidelity. Similar behavior was observed by Huňady et al. [9], who attributed reduced variance in fatigue testing to digital control retrofits in legacy UTMs. Specimen 1 (the blue curve) demonstrates that the original system was unable to maintain stable force control at elevated temperatures, which resulted in excessive ripples and, hence, led to unreliable data. Specimen 2 (the red curve) from the upgraded machine shows clear, stable behavior, indicating that the new load cell and control system can accurately track stress and strain even under thermal stress. Although cast iron is generally brittle, under elevated temperatures (like 150 °C), it may exhibit plasticity before fracture. In this region, the material undergoes permanent deformation, and the testing machine must apply an incessantly steady load to maintain strain. This phase normally demands high force resolution, stable feedback control, and accurate strain tracking. Any instability in the system becomes amplified here, especially for materials with low ductility and abrupt failure modes. The ripple observed in Specimen 1 (before upgrade) is a result of dynamic instability in the force application and measurement system. At 150 °C, the load cell may experience thermal expansion, alter resistance, and cause fluctuating readings. These oscillations are seen as ripples in the stress-strain curve. The other reason for this behavior was the outdated previous motherboard, which had slower sampling rates and less precise PID control, which led to delayed corrections to force and displacement. In the upgraded system, e(t) is minimized continuously, which allows the machine to apply force smoothly even in the sensitive plastic region, without overshooting or oscillation. The mechanical performance of cast iron specimens tested using the upgraded Universal Testing Machine demonstrated notable improvements in stability and measurement fidelity. Reduced undulation and slippage, particularly under elevated temperature conditions, contributed to more consistent stress–strain behavior. As shown in Table 7, elongation increased by 13.62%, indicating enhanced ductility and reduced premature fracture. Additionally, the test time to break was extended by approximately 50%, reflecting improved load control and thermal resilience. The ultimate tensile strength also rose by 1.5%, suggesting more accurate force acquisition and reduced signal noise. From a scientific perspective, the observed improvements in mechanical properties, such as increased elongation, longer time to break, and slightly higher ultimate strength, can be attributed to enhanced load stability, sensor precision, and vibration damping introduced by the upgraded system. These upgrades reduce signal noise, minimize slippage and thermal drift, and ensure more accurate force application throughout the test. As a result, the specimen experiences a more uniform stress field, allowing its intrinsic ductility and strength to be measured more faithfully. Table 9 provides a direct performance benchmark between the original and upgraded machines.

Table 7: As received, test data for the cast iron specimens using the modified machine

No.	Tensile Stress (MPa)	Strength Upper Yield (MPa)	Yield Strength Rp 0.2 (MPa)	Force Peak (kN)	Force Upyield (kN)	Force Down Yield (kN)
1	390.0105	293.4586	369.3185	7.0202	5.2823	5.2825
2	395.6656	376.3793	374.832	7.1228	6.7748	6.747
Max	395.6656	376.3793	374.832	7.1220	6.7748	6.747
Min	390.0105	293.4586	369.3185	7.0202	5.2823	5.2825
Mean	392.8380	334.9189	372.0752	7.0711	6.0286	6.0147

Table 8: As received, test data for the cast iron specimens using the modified machine

No.	Elong. (mm)	Strength Break (MPa)	Force Break (kN)	Tensile Strength (N/mm)	Absorbed Energy (kgf.mm)	Area (mm^2)
1	10.2462	239.7072	4.3147	719.1217	5534.124	18
2	11.6419	220.0177	3.9603	660.0531	6696.891	18
Max	11.6419	239.7072	4.3147	719.1217	6696.891	-
Min	10.2462	220.0177	3.9603	660.0531	5534.124	-

Mean	10.9405	229.8624	4.1375	689.5874	6115.507	-

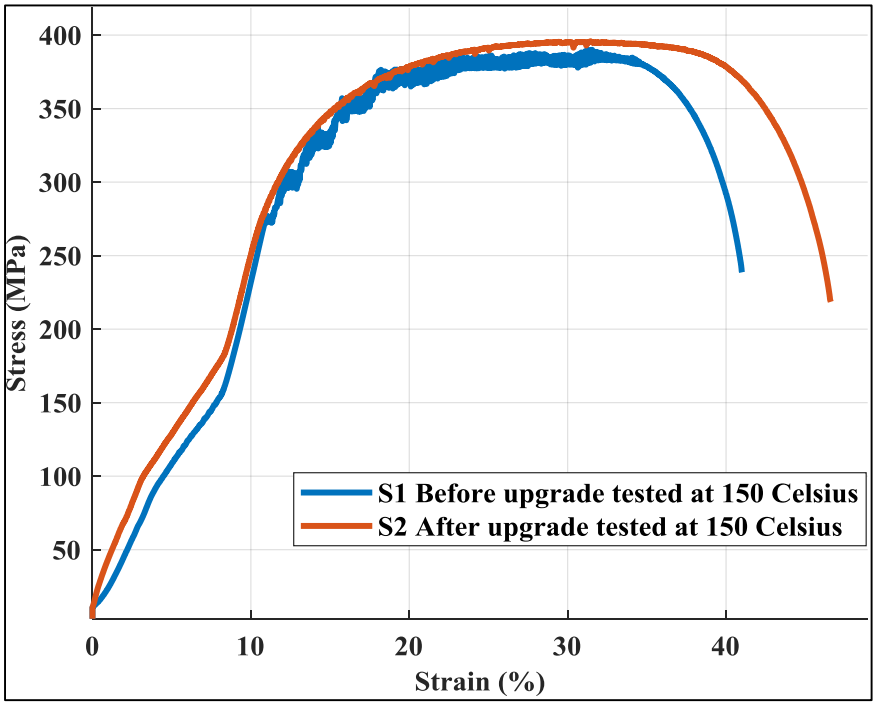

Figure 14 Performance comparison of the machine performance pre and post modification. Specimen 1 (S1) demonstrated an excessive amount of Ripple, slippage, and instability at high temperature. These issues vanished after modification, as shown in specimen 2 (S2), showing a 13.62% increase in elongation.

Table 9: Performance comparison pre- and post-upgrades

Factor	Before Upgrade	After Upgrade
Load Cell	Thermally unstable	Thermally compensated
Servo Motor	Low torque resolution	High torque precision
Control System	Slow, lagging feedback	Fast, real-time control
Ripple in Plastic Region	High	Minimal

Ductile iron is widely used in the petroleum industry for manufacturing pumps. As depicted in Figure 15, specimens of ISO 1030 ductile iron were tested both before and after the machine modification to validate the feasibility of the modification. Specimens 1 and 2, representing specimens tested at 175°C and 200°C before the upgrade, exhibit visible ripples and instability, particularly in the plastic region. This ripple is a result of mechanical and electronic instability in the older testing system. The causes of ripple are due to the load cell instability. At elevated temperatures, the original load cell likely experienced thermal drift, causing erratic force readings. Spcimen3, on the other hand, representing the specimen tested at 200 °C after the upgrade, is smooth and continuous, indicating stable force application and accurate strain tracking. The reasons for improved performance are due to high-resolution load cells. The upgraded sensor is thermally compensated and more precise. The other reason is the responsive servo motor; the new motor delivers consistent force without overshooting or lagging. The real-time upgraded motherboard minimizes errors in the control loop. Specimen 3 curve reaches a higher strain compared to specimens 1 and 2. This is due to both machine capability and material response. The full deformation range was recorded without premature termination. Accurate strain tracking and stable grips, and accurate sensors allow the material to deform naturally. Comparing specimen 2 (200 °C) and 1 (175 °C) curves, the specimen tested at the higher temperature shows greater strain. This is consistent with the thermal behavior of ductile iron. Higher temperatures reduce internal resistance to deformation. Compared to Demmel's open-source UTM [18], which prioritizes accessibility for educational use, our system demonstrates superior performance in high-load industrial testing. While Demmel's design supports basic tensile evaluation, it

lacks the structural reinforcement and sensor resolution required for petroleum-grade material analysis. Our results also surpass those of Mathew and Francis [13], whose modular UTM was validated for low-load applications but did not address industrial reliability or repeatability. According to Tables 10 and 11, the modification resulted in significant improvements in the properties of specimen 3, specifically yield strength and elongation, achieving 12.85mm maximum elongation, which is about 12.8% higher than the first and second specimens before upgrading. Another significant improvement in the YTS was observed, with an improvement of 27.6%. The stable performance of the new load cell under high temperature and the adequate gripping force resulted in accurate force measurements, as the machine was able to achieve a stable pull without stressing and exceeding the rated value of the drive. All these factors combined led to a lower error rate and more reliable results. Table 12: presents performance comparison pre- and post-upgrades.

Table 10: As-received test data for the ductile iron specimens generated by the modified machine.

No.	Tensile Stress (MPa)	Strength Upper Yield (MPa)	Yield Strength Rp0.2 (MPa)	Force Peak (kN)	Force Upyield (kN)	Force Down Yield (kN)
1	268.1193	215.1852	145.0186	4.8261	3.8733	2.6103
2	257.4682	181.5701	132.5424	4.6344	3.2683	2.3858
3	264.3438	190.7012	169.1375	4.7582	3.4326	3.0445
Max	268.1193	215.1852	169.1375	4.8261	3.8733	3.0445
Min	257.4682	181.5701	132.5424	4.6344	3.2683	2.3858
Mean	263.3104	195.8188	148.8995	4.7396	3.5247	2.6802

Table 11: As-received test data for the ductile iron specimens generated by the modified machine.

No.	Elong.	Strength break (MPa)	Force Break (kN)	Tensile strength (N/mm)	absorbed energy (kgf.mm)	Area (mm^2)
1	11.40	137.2495	2.4705	411.7486	4487.412	18
2	12.06	129.4151	2.3295	388.2453	4677.281	18
3	12.85	132.8365	2.3911	398.5096	5130.741	18
Max	12.85	137.2495	2.4705	411.7486	5130.741	-
Min	11.40	129.4151	2.3295	388.2453	4487.412	-
Mean	12.103	133.167	2.397	399.5012	4765.145	-

Table 12: Performance comparison pre- and post-upgrades

Factor	Before Upgrade	After Upgrade
Curve Stability	Rippled, unstable	Smooth, continuous
Max Strain	Moderate	Slightly increased
Load Cell	Thermally unstable	Thermally compensated
Feedback Control	Lagging	Real-time, responsive
Temperature Effect on Performance	Extreme	Contained and controlled

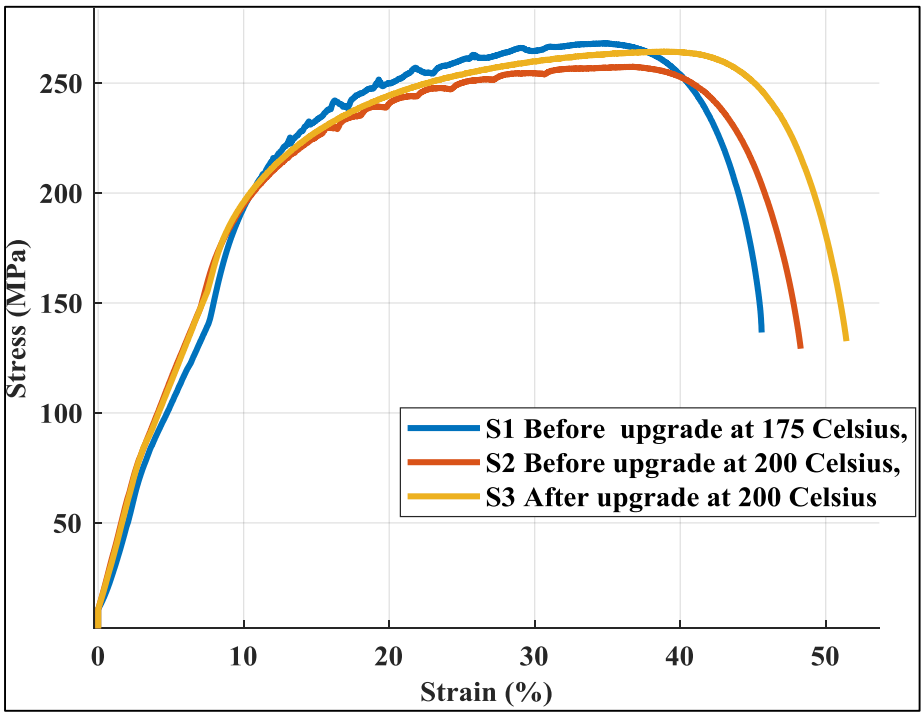

Figure 15: Performance comparison of the machine performance pre and post modification. Stress-strain curves for the ductile iron material were generated by the modified machine. S3, the updated performance showed smoothness, stability, and a dramatic reduction in slippage and undulation during testing at high temperatures.

The original mounting system lacked sufficient damping capacity, allowing mechanical oscillations to propagate through the load frame. These vibrations were mainly problematic during the elastic to plastic transition phase of tensile tests, where precise force resolution is essential. Figure 16 represents the time domain waveform of the machine vibration level at room temperature before and after the upgrade. Accelerometer-based vibration measurements confirmed that the system before the upgrade system exhibited peak vibration amplitudes exceeding 0.318 g 3.115 m/s^2, well within the bandwidth of the original 20 kn load cell, thus contaminating the signal. Post-upgrade accelerometer readings showed a reduction in peak vibration amplitude by about 70%, with most oscillations dampening below 0.1 g 1.256 m/s^2. The dominant frequencies were shifted outside the sensitive range of the load cell, resulting in cleaner, more stable force-displacement curves. This improvement is consistent with findings from Huňady et al [9], who demonstrated that digitized and structurally reinforced UTMs exhibit significantly lower signal noise and improved fatigue test repeatability. Vibration damping plays a critical role in ensuring the repeatability of mechanical tests, particularly in industrial environments where ambient disturbances and machine-induced oscillations are common. Over extended testing periods, even minor vibrations can introduce noise into sensor readings, affect load stability, and compromise the accuracy of strain measurements. In our upgraded system, the integration of reinforced structural supports and elastomeric damping elements significantly reduced mechanical resonance during operation. This contributed to a measurable decrease in inter-test variance post-modification. Such improvements are essential in petroleum-sector applications, where consistent material evaluation under high-load conditions directly influences component reliability and operational safety.

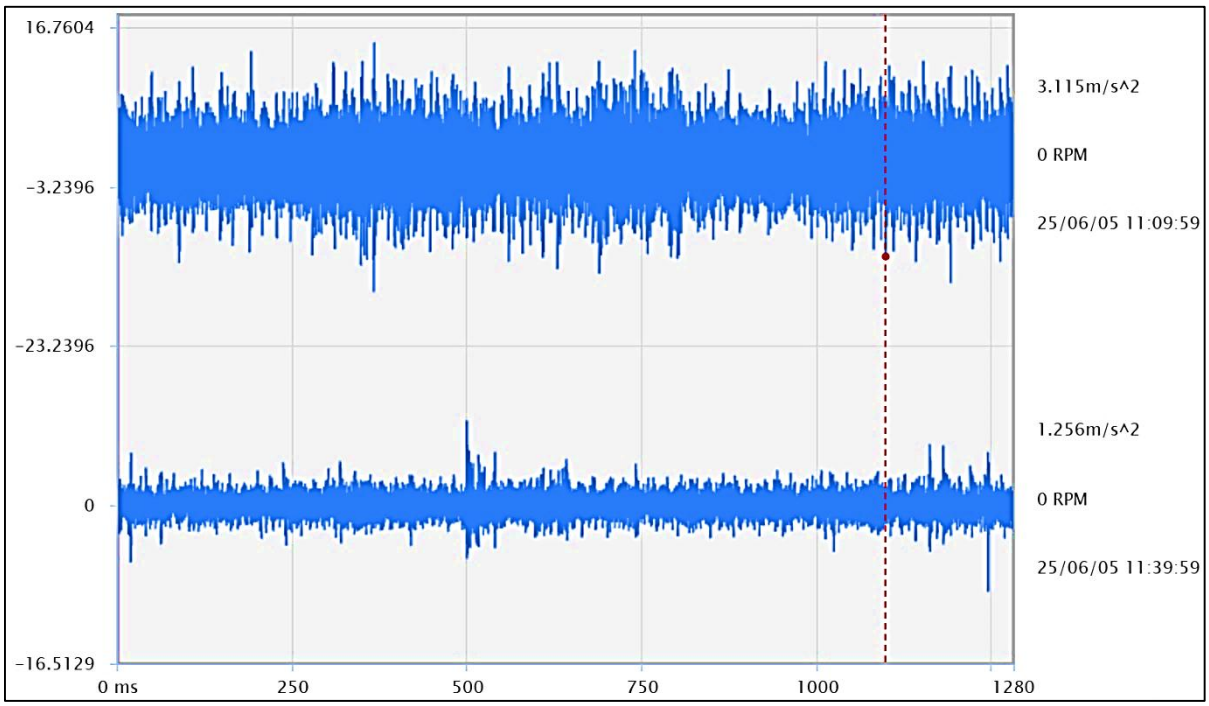

Figure 16: Focused time domain row signal post and before the upgrade, illustrating the vibration reduction. This figure indicates a significant amount of vibration reduction after modification. Where the y-axis represents the acceleration, and the x-axis represents time in milliseconds

In practical terms, the upgraded Universal Testing Machine offers a compelling balance of cost-efficiency, reliability, and operational speed compared to commercial systems. While high-end industrial UTMs typically cost between $25,000 and $60,000 USD, as shown in Table 13, our modified system was developed for under $8,000 USD, including sensor upgrades and control integration. Reliability was assessed through repeated testing over 6 months, during which the system maintained consistent performance with minimal recalibration, comparable to commercial-grade machines. In terms of time efficiency, the upgraded UTM reduced setup and calibration time, owing to its streamlined interface and modular design. These practical advantages make the system particularly suitable for mid-scale industrial labs and maintenance operations in the petroleum sector, where budget constraints and testing throughput are critical.

Table 13: Practical Comparison of UTM Systems

Feature	Upgraded UTM (This Study)	Commercial UTM (e.g., Instron, MTS)
Approximate Cost	<$8,000 USD	$25,000–$60,000 USD
Reliability (6 months)	Stable, minimal drift	Stable, auto-calibrated
Calibration Frequency	Monthly manual check	Automated or quarterly
Setup Time	~15 minutes	~25–30 minutes
Test Throughput	Moderate (10–15/day)	High (20–30/day)
Maintenance Cost	Low	Moderate to high

Note: Commercial benchmarks based on published specs and vendor documentation.

5. Conclusions

The upgraded Universal Testing Machine (UTM) developed in this study significantly enhances measurement accuracy, repeatability, and operational efficiency, making it well-suited for evaluating materials used in petroleum centrifugal pumps. By increasing servo power from 750 W to 2000 W, the system achieved a 166% boost in load capacity, enabling reliable tensile testing of high-strength materials like SS316, 1018 steel, A514 Alloy Steel, cast iron, and ductile iron, previously prone to slippage and stalling. The new 50 kN load cell maintained stable readings up to 300 °C, reducing drift and improving high-temperature performance by 50% over the prior 20 kN unit, with percentage errors typically between 1.6–2%. Custom wedge grips designed to ASTM E8/E8M standards eliminated slippage under high loads, achieving just 2% error in elongation measurements.

Rubber mounts reduced frame vibrations by over 75%, enhancing signal stability, an approach consistent with established damping practices in precision equipment. Compared to the benchmark system, the upgraded UTM demonstrated superior stability, accuracy, and mechanical synchronization, capturing full plastic deformation curves even for high-strength materials. Economically, the system offers an 86% cost reduction, with a total build cost under $8,000 USD versus $25,000–$60,000 USD for commercial alternatives, making it ideal for mid-scale industrial labs. Long-term reliability was confirmed over six months of repeated high-temperature testing, with minimal recalibration and stable inter-test variance of ±5 MPa. While the system currently supports tensile and compression testing, it lacks modules for fatigue and impact. Incorporating a high-temperature extensometer would further improve strain rate measurement and expand testing capabilities.

Conflict of Interest: The authors declare that they have no conflict of interest.

References

[1] Wigley D. Mechanical properties of materials at low temperatures. Springer Science & Business Media; 2012 Dec 6.

[2] Merklein M, Biasutti M. Development of a biaxial tensile machine for characterization of sheet metals. Journal of Materials Processing Technology. 2013 Jun 1;213(6):939-46.

[3] Qualitest, “Universal testing machines: Comprehensive overview—basics & applications,” World of Test, 2024. [Online]. Available: https://www.worldoftest.com/articles/universal-testing-machines-comprehensive-overview-basics-applications

[4] M. Rizal, U. Aulia, and R. Yudiansyah, “Development of a Portable Universal Testing Machine for Investigating the Mechanical Properties of Medium-Strength Materials,” Aceh Int. J. Sci. Technol., vol. 12, no. 1, Apr. 2023.

[5] L. Abatta-Jácome, J. Arboleda-Álvarez, M. Chiluiza-Pullupaxi, and E. E. Haro, “Design and construction of a low-cost and low-scale universal testing machine for tensile test,” in Proc. XV Multidisciplinary Int. Congr. Sci. Technol., Cham, Switzerland: Springer Int. Publishing, Jun. 14, 2021, pp. 135–150.

[6] Jasim MF, Abbas TF, Huayier AF. The effect of infill pattern on tensile strength of PLA material in fused deposition modeling (FDM) process. Engineering and Technology Journal. 2022 Sep 25;40(21):1723-30.

[7] O'CONNOR GE. Development of high high-temperature tensile test machine (Doctoral dissertation, University of Limerick).

[8] Waheed MS, Hafad SA. Study of tensile strength and compression strength of binary polymeric blends (High-Density polyethylene/polycarbonate). Eng. &Tech. 2008;26(7).

[9] Huňady R, Sivák P, Delyová I, Bocko J, Vavro Jr J, Hroncová D. Upgrade of the universal testing machine for the possibilities of fatigue tests in a limited mode. Applied Sciences. 2024 May 7;14(10):3973.

[10] Huerta E, Corona JE, Oliva AI, Avilés F, González-Hernández J. Universal testing machine for mechanical properties of thin materials. Revista mexicana de física. 2010 Aug;56(4):317-22.

[11] Lim W, Kim HK. Design and development of a miniaturised tensile testing machine. Global journal of engineering education. 2013;15(1):48-53.

[12] Baker BW. Processing, microstructure, and material property relationships following friction stir welding of oxide dispersion strengthened steels (Doctoral dissertation, Monterey, California: Naval Postgraduate School).

[13] S. Mathew and V. Francis, Development, Validation and Implementation of Universal Testing Machine, Jönköping University, Sweden, pp. 6–7, 2019.

[14] Ghadhban TY, Al-ALkawi HJ, Reja AH. Design, Fabrication, and Testing of an Electromechanical High-Temperature Tensile Test Machine.

[15] Abatta-Jácome L, Arboleda-Álvarez J, Chiluiza-Pullupaxi M, Haro EE. Design and construction of a low-cost and low-scale universal testing machine for tensile test. InXV Multidisciplinary International Congress on Science and Technology 2021 Jun 14 (pp. 135-150). Cham: Springer International Publishing.

[16] Moayyedian M, Qazani MR, Cvorovic V, Asi F, Mussin A, Hedayati-Dezfooli M, Dinc A. Tensile Test Optimization Using the Design of Experiment and Soft Computing. Processes. 2023 Oct 30;11(11):3106.
[17] Senthil Kumar J, Surya B, Arjun VS. Micro universal testing machine system for material property measurement of microstructure. In AIP Conference Proceedings 2024 Mar 4 (Vol. 3035, No. 1, p. 020002). AIP Publishing LLC.
[18] S. Demmel, Design, Manufacturing, and Testing of an Open-Source Universal Testing Machine for Hands-On Learning [Diploma Thesis], Technische Universität Wien, 2024. [Online]. Available: https://doi.org/10.34726/hss.2024.113842
[19] Nwigbo MN, Gwarah BG, Gwarah PN. Design, Fabrication and Performance Evaluation of a Tensile Testing Machine.
[20] F. P. Beer, E. R. Johnston, J. T. DeWolf, and D. F. Mazurek, Mechanics of Materials, 7th ed. New York, NY, USA: McGraw-Hill Education, 2015, pp. 35–36.
[21] R. C. Hibbeler, Engineering Mechanics: Dynamics, 14th ed. Upper Saddle River, NJ, USA: Pearson Education, 2016, pp. 380–382.Available: https://scholar.google.com/scholar_lookup?title=Mechanics+of+Materials&author=Beer&publication_year=2015 https://scholar.google.com/scholar_lookup?title=Engineering+Mechanics:+Dynamics&author=Hibbeler&publication_year=2016
[22] W. F. Hosford, Mechanical Behavior of Materials, 2nd ed. Cambridge, UK: Cambridge University Press, 2010, pp. 97–99. Available: https://scholar.google.com/scholar_lookup?title=Mechanical+Behavior+of+Materials&author=Hosford&publication_year=2010
[23] K. Ogata, Modern Control Engineering, 5th ed. Upper Saddle River, NJ, USA: Prentice Hall, 2010, pp. 110–112. Available: https://scholar.google.com/scholar_lookup?title=Modern+Control+Engineering&author=Ogata&publication_year=2010
[24] [6] J. G. Webster, Measurement, Instrumentation, and Sensors Handbook, 2nd ed. Boca Raton, FL, USA: CRC Press, 2014, pp. 3–5. Available: https://scholar.google.com/scholar_lookup?title=Measurement,+Instrumentation,+and+Sensors+Handbook&author=Webster&publication_year=2014
[25] D. C. Montgomery and G. C. Runger, Applied Statistics and Probability for Engineers, 7th ed. Hoboken, NJ, USA: Wiley, 2018, pp. 36–38. Available: https://scholar.google.com/scholar_lookup?title=Applied+Statistics+and+Probability+for+Engineers&author=Montgomery&publication_year=2018